Journal of ELECTRONIC MATERIALS, Vol. 46, No. 5, 2017
DOI: 10.1007/s11664-016-5155-4

Optimization of Heat Exchangers with Dimpled Surfaces to Improve the Performance in Thermoelectric Generators Using a Kriging Model

SHUAI LI,[1] YIPING WANG,[1,2,4] TAO WANG,[1] XUE YANG,[3] YADONG DENG,[1] and CHUQI SU[1]

1.—Hubei Key Laboratory of Advanced Technology for Automotive Components, Wuhan University of Technology, Wuhan 430070, China. 2.—Hubei Collaborative Innovation Center for Automotive Components Technology, Wuhan University of Technology, Wuhan 430070, China. 3.—Wuhan Ordnance Noncommissioned Officers School, Wuhan 430075, China. 4.—e-mail: wangyiping@whut.edu.cn

Thermoelectric generators (TEGs) have become a topic of interest for vehicle exhaust energy recovery. Electrical power generation is deeply influenced by temperature differences, temperature uniformity and topological structures of TEGs. When the dimpled surfaces are adopted in heat exchangers, the heat transfer rates can be augmented with a minimal pressure drop. However, the temperature distribution shows a large gradient along the flow direction which has adverse effects on the power generation. In the current study, the heat exchanger performance was studied in a computational fluid dynamics (CFD) model. The dimple depth, dimple print diameter, and channel height were chosen as design variables. The objective function was defined as a combination of average temperature, temperature uniformity and pressure loss. The optimal Latin hypercube method was used to determine the experiment points as a method of design of the experiment in order to analyze the sensitivity of the design variables. A Kriging surrogate model was built and verified according to the database resulting from the CFD simulation. A multi-island genetic algorithm was used to optimize the structure in the heat exchanger based on the surrogate model. The results showed that the average temperature of the heat exchanger was most sensitive to the dimple depth. The pressure loss and temperature uniformity were most sensitive to the parameter of channel rear height, h_2. With an optimal design of channel structure, the temperature uniformity can be greatly improved compared with the initial exchanger, and the additional pressure loss also increased.

Key words: TEG, heat exchanger, dimpled surface, optimization, Kriging model

INTRODUCTION

For transportation vehicles powered by combustion engines, about 40% of the energy is lost through gas emission waste. With the rapid development of semiconductor materials, thermoelectric generators (TEGs) as a useful technique can directly convert thermal energy into electrical energy in automobile applications. Researchers[1–4] have reported that several hundreds of watts of power can be generated in different experimental conditions when installing the device in the vehicle exhaust. Previous studies have shown that improving the heat exchanger could extract more power. The electrical power generation is deeply influenced by temperature differences, temperature uniformity and the topological structure of the TEG.

(Received June 12, 2016; accepted November 16, 2016; published online November 30, 2016)

Sarhadi et al.[5] took into account the contact pressure, roughness and hardness of the interface surfaces as well as the air gap thermal resistance at the interface in the TEG, and evaluated the power production of the integrated system using different interface materials, including graphite, aluminum (Al), tin (Sn) and lead (Pb) in a form of thin foils. The numerical results showed that lead foil at the interface had the best performance. Sidek and Ishak[6] investigated the influence of the material properties on the temperature uniformity, the results revealing that copper gives the most uniform temperature distribution. Jang and Tsai[7] improved the temperature uniformity by optimizing the spreader thickness; the results showed that the maximum power P_{max} could be significantly increased (by up to 50%). It is undeniable that the temperature uniformity could be improved by employing different materials and modifying the structure of the exchanger, but it should be noted that these methods were empirical. Zhang and Cleary[8] conducted an optimum design of the heat exchanger by the aid of a computational fluid dynamics (CFD) model and obtained a maximum heat transfer rate with minimum pressure drop. Kim and Son[9] performed a numerical study for a tubular heat exchanger to evaluate the effect of the optimum arrangements of guide vanes in a combining header on the performance of the heat exchanger. The Pareto analysis results indicated that the total pressure drop and the flow uniformity of the heat exchanger were inversely related. Mohanty[10] applied the Firefly algorithm to obtain an optimal design for a shell and tube heat exchanger in industrial applications. Cavazzuti et al.[11] presented a numerical application in a finned concentric pipes heat exchanger for industrial recuperative burners. It was found that the fine tuning of just a few geometrical parameters can result in a sensible enhancement of the exchanger efficiency. Lee and Kim[12] optimized arc-shaped ribs in the cooling channels of a printed circuit heat exchanger to enhance heat transfer and also reduce the pressure drop. The optimal designs showed large increases in both the thermal performance and pressure drop compared to the reference design without ribs. Quan et al.[13] optimized the electric topology of thermoelectric modules using a genetic algorithm to achieve the maximum peak power of the automobile exhaust TEG. Due to the different voltage and current characteristics of each thermoelectric module, if they are all connected in series, the output current of the TEG is restricted by the one with the minimum temperature difference. If a number of modules with different open-voltage values are connected in parallel, there will be a ring current between them, as their final output voltage has to be the same, which will increase the internal power loss. In their research, all the thermoelectric modules with the same or similar open-circuit voltage values were connected in parallel as a basic voltage element so that little ring current existed between them, which involved a complex connection between the thermoelectric modules. A similar working state of each thermoelectric module is important to improve power generation from the TEG. Wang et al.[14] and Su et al.[15] both adopted optimization methods to modify the structure distribution of the heat exchanger with fins or a folded-shaped structure to increase its temperature uniformity. Their researches optimized the structure parameters and prevented an empirical adjustment on the heat exchanger.

Wang et al.[16] present a mathematical model to simulate the impact of relevant factors, e.g., the vehicle exhaust mass flow rate, temperature and mass flow rate of different types of cooling fluid, convection heat transfer coefficient, on the output power and efficiency. Their research revealed that output power and efficiency could be improved by increasing the convection heat transfer coefficient of the high-temperature side but that this method is costly due to the limited space and back-pressure of the exhaust. Dimples have been demonstrated to be a useful structure in solving many engineering problems such as vehicle drag reduction,[17] noise elimination,[18] and heat transfer enhancement.[19] Wang et al.[20] firstly used the dimples in the heat exchanger of a vehicle TEG, and the results showed that the heat transfer was enhanced and the back-pressure was relatively low. However, the fluid temperature decreased rapidly in the downstream direction in the heat transfer process, which influenced the temperature uniformity. Previous work had shown that the temperature uniformity led to improved power from the TEG, and that the introduction of a dimpled surface enhanced the heat transfer, but with the thermal energy extracted from the exhaust, the fluid temperature decreased rapidly in the downstream direction. This rapid decrease influenced the surface temperature uniformity which was related to the thermoelectric efficiency and generation capacity. Therefore, it makes sense to conduct the related research to enhance the downstream heat transfer in order to improve the heat uniformity of the exchanger.

An optimization study was conducted to improve the temperature uniformity of a heat exchanger with a dimpled surface. For the channel structure, four factors were considered: dimple depth, dimple print diameter, channel front height and channel rear height. Based on these four factors, a design of experiments (DOE) study using the optimal Latin hypercube experimental method was conducted to analyze the sensitivity of the design variables and to build a database to set up a surrogate model using the Kriging response surface method. Finally, a multi-island genetic algorithm was used to optimize the channel structure based on this surrogate model.

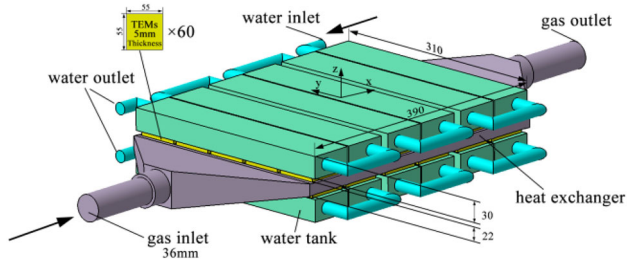

Fig. 1. Schematic model of TEG (unit: mm).

COMPUTATIONAL METHOD AND PROCEDURE

Geometry and Meshing

The automotive TEG consists of a heat exchanger, coolant and thermoelectric modules. Its configuration is shown in Fig. 1, in which 12 rows of thermoelectric modules (TEMs) acan be seen mounted on the top and the bottom surfaces of the heat exchanger. The entry and exit ports of the box are connected to the exhaust pipe of the automobile. To ensure a cooling effect, the flow direction in the water tank was opposite to the direction of the exhaust. The coordinate origin was located in the center of the heat exchanger. Thanks to the temperature difference between the top and bottom of thethermoelectric modules, heat is directly converted into electricity.

The exchanger segment was a rectangular channel, 305 mm in width and 400 mm in length (see Fig. 2), and the wall thickness of the heat exchanger was 5 mm. The fins (at the front end) and the deflectors can maintain the uniformity of the flow field, and support the structural strength of the heat exchanger. To enhance the heat transfer performance and surface temperature uniformity, there is a symmetrical arrangement of dimpled surfaces staggered on the interior surface of the heat exchanger. To increase the area of convective heat transfer which is helpful to enhance the rear section temperature, some cylinder fins 16 mm in diameter have been set in the rear section of the exchanger segment. Moreover, the heat exchanger surfaces can be parallel or not, in order to allow that the fluid flows gradually faster which could contribute to a heat transfer enhancement in the downstream direction. Thus, the temperature uniformity was improved because of a balance between the fluid temperature and the heat transfer coefficient. Dimple depth (S), dimple print diameter (D), channel front height (h_1) and channel rear height (h_2) were selected with parameterized modeling to conduct further optimization (see Fig. 2).

All the computational meshes were tetrahedral unstructured meshes and generated in ICEM-CFD. A grid dependence study was conducted on the initial design model (D = 15 mm, S = 3 mm, h_1 = 12 mm, h_2 = 12 mm). To check mesh convergence, three mesh strategies were employed: 3.0

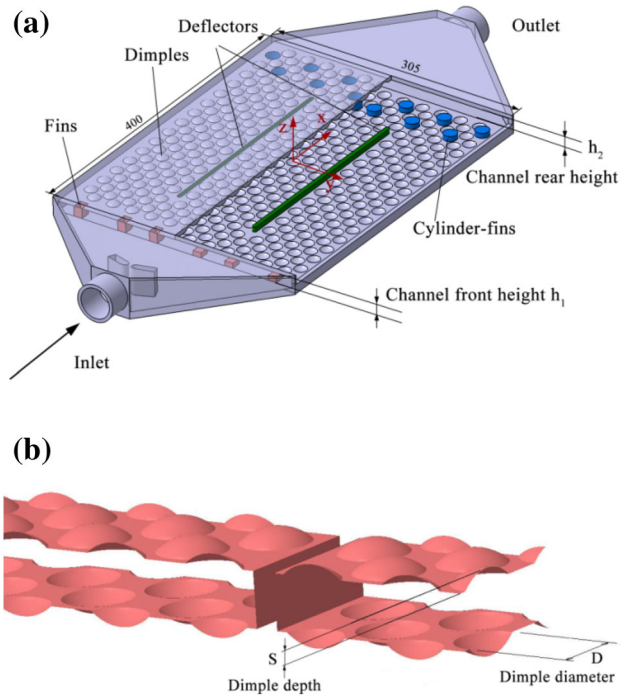

Fig. 2. (a) Schematic model of heat exchanger; (b) schematic model of dimples (unit: mm).

million for the coarse mesh, 4.5 million for the fine mesh and 6.5 million for the finer mesh. The wall normal resolution was $y+ < 0.3$, $y+ < 1$, $y+ < 3$ of the fine mesh, the middle mesh and the coarse mesh, respectively. Here, $y+ = \Delta y \mu\tau / v$, Δy is the wall-normal distance, $\mu\tau$ is the friction velocity and v is the kinematic viscosity. In general, the backpressure between all grid systems was very small, and a relative small difference of average temperature was found between the fine mesh and the finer mesh, as shown in Table I. The grid system of about 4.0 M cells was chosen for all computations. For each case, it may need 8 h to reach the required accuracy with four CPUs and 16G storage.

Turbulence Model and Boundary Conditions

A realizable k–ε model was adopted to compute the flow field and heat transfer in the current research. For a three-dimensional steady incompressible flow, the conservation equations for mass, momentum, and energy are defined as follows,

Continuity equation:

$$\frac{\partial \rho}{\partial t} + \nabla \cdot \left(\rho \overrightarrow{W} \right) = 0 \tag{1}$$

Momentum equation:

$$\frac{\partial \rho \overrightarrow{W}}{\partial t} + \nabla \cdot \left(\rho \overrightarrow{W} \times \overrightarrow{W} + P[I] \right) - \nabla \cdot ([\tau]) + \rho \left[2\vec{\omega} \times \overrightarrow{W} + \vec{\omega} \times \left(\vec{\omega} \times \vec{\gamma} \right) \right] = 0 \tag{2}$$

Table I. Grid dependence study

	Coarse (3.0 M)	Fine (4.5 M)	Finer (6.5 M)
Average temperature	581.89	581.12	581.05
Pressure loss	1703	1681	1685
Temperature difference	0.9260	0.9262	0.9260

Energy equation:

$$\frac{\partial \rho E}{\partial t}+\nabla\cdot\left(\rho E\overrightarrow{W}+P[I]\cdot\overrightarrow{W}\right)-\nabla\cdot\left(k\nabla T+[\tau]\cdot\overrightarrow{W}\right)-\rho\nabla\left(\frac{\omega^2 r^2}{2}\right)\cdot\overrightarrow{W}=0 \tag{3}$$

where the ρ is the density, P is the static pressure of the fluid and $\overrightarrow{W}$ is the relative velocity vector of the fluid. $[I]$ and $[\tau]$ are, respectivelys the unit tensor and viscous stress tensor of the fluid, E is the total energy of unit mass flow, ω is the rotational speed of the relative coordinate system, k is the thermal conductivity of the fluid and T is the static temperature.

The simulation process is based on the experiment on the test bench. As shown in Ref. 24 for simulation boundary conditions, a uniform mass flow inlet was set at 0.033 kg/s and the air temperature was fixed at 673 K. A turbulence intensity of 5% and hydraulic diameter at 0.036 m were chosen as turbulence quantities for the inlet. Because there was a rear muffler next to the heat exchanger, considering the back-pressure produced by muffler varied from 4000 Pa to 6000 Pa, the pressure at the outlet of the heat exchanger was set as 5000 Pa. In the natural convection process, the convective heat transfer coefficient between the outer surface and circumstance air varies from 10 W/(m^{2}K) to 25 W/(m^{2}K). A uniform heat transfer coefficient at a value of 20 was applied over all the surface of the heat exchanger. No-slip velocity conditions were applied on all walls. Indeed, due to the importance of secondary flow and impact flow to the heat transfer, enhanced wall treatment was employed for the near-wall treatment. The fluid in the current research was incompressible dry air and assumed to have constant thermal physical properties, while its physical values have to be modified, such as density, specific heat, and thermal conductivity. A least squares cell-based and standard discretized schemes were selected for the gradient and pressure respectively. The second-order upwind was selected for momentum, turbulent kinetic energy, turbulent dissipation rate and energy. The minimum convergence error criterion for the energy equation was 10^{-7}, while 10^{-4} was chosen for the continuity equation and momentum equation.

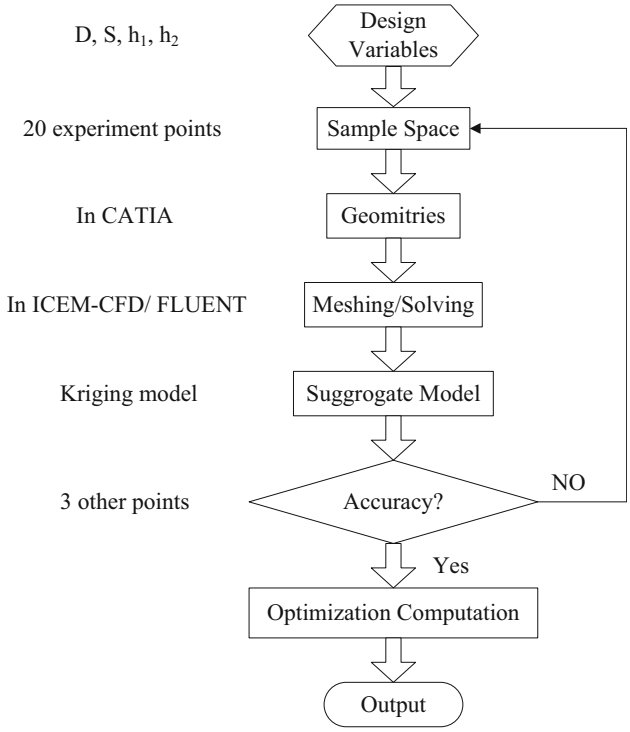

Fig. 3. Optimization process.

OPTIMIZATION DESIGN

Design Variables and Objective Function

To increase the temperature and improve its uniformity in the current study, a dimpled structure was installed in the heat exchanger. Structural parameters such as dimple depth (S), dimple print diameter (D), channel front height (h_1) and channel rear height (h_2) were optimized. The integrated process for the heat exchanger optimization is plotted in Fig. 3. In an appropriate DOE method, the optimal Latin hypercube method was employed to build a database for the heat exchanger by using different values of S, D, h_1, and h_2.

After the DOE process, numerical simulations were conducted to obtain the average temperature, pressure drop and temperature uniformity. In this study, to evaluate the temperature uniformity of the heat exchange area, the temperature uniformity coefficient γ is defined by:

$$\gamma=1-\frac{1}{\sqrt{n}}\sum_{i=1}^{n}\frac{\sqrt{(T_i-T_{\text{mean}})^2}}{T_{\text{mean}}} \tag{4}$$

where n is the number of TEMs, T_i is the temperature at each TEM center and T_{mean} is the average temperature of the heat exchange surface. When the temperature of all the measurement points is the same, γ is equal to 1, which implies that the temperatures of the heat transfer surfaces are the most uniform.

Pressure drop is defined as the difference between the inlet and outlet pressures of the heat exchanger. The pressure drop is calculated by the following equation:

$$P_{\text{drop}} = P_{\text{in}} - P_{\text{out}} \tag{5}$$

where P_{drop} is the pressure drop along the heat exchanger. P_{in} is the area-averaged pressure of the inlet and P_{out} is the area-averaged pressure of the outlet.

Based on the simulation results with different S, D, h_1, and h_2 values, a surrogate model was set up by using the Kriging method according to the inputs and corresponding outputs. Then, the multi-island genetic algorithm was used to determine the optimum using this surrogate model to evaluate the objective functions and constraints.

For this process, considering that the average temperature and pressure drop for the initial heat exchanger are, respectively, 581.12 K and 1681 Pa, it is hoped to maintain the average temperature and to control the pressure at an acceptable value. The average pressure loss of 20 experiment points was 1743 Pa. In order to obtain a best temperature uniformity, the objective function is defined as the following forms:

$$\max\ \gamma(p_1, p_2, p_3, p_4) \tag{6}$$

$$T(p_1, p_2, p_3, p_4) \geq 581 \tag{7}$$

$$P_{\text{drop}}(p_1, p_2, p_3, p_4) \leq 1743 \tag{8}$$

$$\text{s.t. } p_1 \in X_1, \quad p_2 \in X_2, \quad p_3 \in X_3, \quad p_4 \in X_4 \tag{9}$$

which are to minimize the temperature difference and control the average temperature as well as the pressure loss. The parameters p_1, p_2, p_3, and p_4 are the values of the design variables and refer to the dimple depth S, dimple diameter D, channel front height h_1 and channel rear height h_2, respectively. The parameters X_1, X_2, X_3, and X_4 are the design spaces of the design variables. To avoid the geometry interference and keep the dimples hemi-spherical, the ranges of X_1, X_2, X_3, and X_4 are set as [0, 4.5], [9,16] [12, 32], and [6, 12]

Optimal Latin Hypercube Design

The optimal Latin hypercube design[21] is a kind of technique in the design of experiments in which the combination of factor levels for each factor is optimized, rather than randomly uniformly divided. These levels are then randomly combined to generate a random Latin hypercube as the initial DOE design matrix with n points. An optimization process is then applied to this initial random Latin hypercube design matrix. By swapping the order of two factor levels in a column of the matrix, a new matrix is generated and the new overall spacing of points is evaluated. The advantage of this optimization process is to design a matrix in which the points are spread as evenly as possible within the design space defined by the lower and upper levels of each factor. Considering that four structural parameters were optimized and 16 experiment points were selected in Ref. 14, in the current study, 20 experiment points were selected with the optimal Latin hypercube method.

Kriging Method

The sample space is only 20 experiment points by the optimal Latin hypercube method. For each experiment point, the heat exchanger model is built and the temperature distribution is simulated. Based on these simulation results, the Kriging method[22] in its basic formulation estimates the value of a function (response) at some unsampled location as a combination of two components, the global model and the asystematic departure, mathematically:

$$y(x) = f(x) + Z(x) \tag{10}$$

where $y(x)$ is the unknown function to be estimated and $f(x)$ is a known function (usually polynomial) representing the trend over the design space, also referred to as the 'global' model. The second part, $Z(x)$, creates a localized deviation to interpolate the sampled data points by quantifying the correlation of the points with a Gaussian correlation having zero mean and nonzero covariance. The covariance matrix of $Z(x)$ is given by

$$\text{cov}\left[Z(x^i), Z(x^j)\right] = \sigma^2 \boldsymbol{R}\left[R(x^i, x^j)\right], \quad (i, j = 1, 2, \ldots, n) \tag{11}$$

where $\boldsymbol{R}$ is a correlation matrix consisting of a spatial correlation function (SCF), with $R(x^i, x^j)$ as its elements. σ^2 is the process variance representing the scalar of the spatial correlation function quantifying the correlation between any two ns sampled data points x^i and x^j, and thereby controls the smoothness of the Kriging model, the effect of nearby points, and differentiability of the surface. The Gaussian function used in this work is the most preferable SCF when used with a gradient-based optimization algorithm, as it provides a relatively smooth and infinitely differentiable surface.

Multi-island Genetic Algorithm Method

The multi-island genetic algorithm method (MIGA)[23] has been developed based on the traditional genetic algorithm (TGA). The main feature of the MIGA is that each population of individual is

divided into several sub-populations called "islands". All traditional genetic operations, such as selection, crossover and mutation, are performed separately on each island. Some individuals are selected from each island and periodically migrated to different islands. During the evolution procedure, two parameters control the migration process: migration interval and migration rate. The migration interval determines the number of generations between each migration, and the migration rate specifies the percentage of individuals migrated from each island. MIGA can avoid the local optimal solution and restrain the chance of premature convergence.

RESULTS AND DISCUSSION

To explore the design space and identify the significant design variables, the 20-level DOE study presented in Table II was conducted using the optimal Latin hypercube method for the channel structure variables. The 20 levels of each design variable were divided between the lower and upper bounds of the design space. With these 20 design points, the parameterized heat exchanger model was updated and meshed, and the temperature distribution was obtained from the CFD simulation. Table II showed the response for average temperature, pressure loss and temperature uniformity, ranging from 567.23 K to 584.93 K, 1582 Pa to 2176 Pa, and 0.9288 to 0.9591, respectively.

Based on the optimization software Isight, Pareto plots for average temperature, pressure loss and temperature uniformity are given in Fig. 4. These take the form of an ordered bar chart of the normalized coefficients, which represent the percentage total effect on the response. The ten parameters (e.g., S and h_1) or interaction effect parameters (e.g., h_1–S and h_1–h_2) which had a significant influence are listed in the plot. The blue bar indicates an active effect and the red bar indicates a negative effect. Figure 4a shows that the effect of S on temperature was approximately 22% and that this parameter had the most active effect on the temperature, which indicates the importance of setting dimples on the interior wall of the heat exchanger. Furthermore, the channel height h_1 had the most negative effect on average temperature. Figure 4 also shows that the channel rear height h_2 had the most negative effect on the pressure loss and temperature uniformity. This means that the lower the channel rear height, the higher the pressure drop and the temperature uniformity.

Based on the DOE and CFD simulation results, a surrogate model using the Kriging method was built. To examine and certify the fitting precision of the surrogate model, another three design points were chosen. The average temperature, pressure loss and temperature uniformity of these three points were compared with the CFD simulation results and the surrogate model estimated values. The results are presented in Table III. The relative error equals the ratio of the absolute error and the CFD simulation result. The absolute error equals the absolute value of the difference between the surrogate model result and the CFD simulation result.

The optimal design variables and objectives were calculated based on the surrogate model and the

Table II. Design matrix and results

	Input variables				Response variables		
Case	D (mm)	S (mm)	h_1 (mm)	h_2 (mm)	T (K)	P (Pa)	γ
1	11	0.24	18	10	569.77	1604	0.9381
2	10	2.84	19	12	573.55	1620	0.9420
3	14	4.26	26	8	578.74	1785	0.9521
4	14	1.89	13	11	578.02	1635	0.9288
5	15	2.13	32	9	570.04	1622	0.9407
6	12	3.32	17	6	584.93	2176	0.9591
7	12	0	28	9	567.23	1605	0.9405
8	12	3.79	30	11	572.51	1613	0.9356
9	16	0.71	21	9	569.39	1684	0.9479
10	13	1.18	27	12	565.82	1582	0.9366
11	11	2.61	31	7	573.10	1768	0.9553
12	9	4.03	23	8	576.90	1783	0.9512
13	9	1.42	29	10	567.81	1611	0.9420
14	10	2.37	12	9	582.95	1812	0.9340
15	16	3.08	15	8	584.59	1912	0.9491
16	13	0.47	14	7	576.99	1864	0.9451
17	10	0.95	20	7	574.23	1848	0.9526
18	15	1.66	25	6	580.60	1885	0.9591
19	13	4.5	16	10	581.35	1768	0.9462
20	15	3.55	24	11	575.99	1684	0.9439

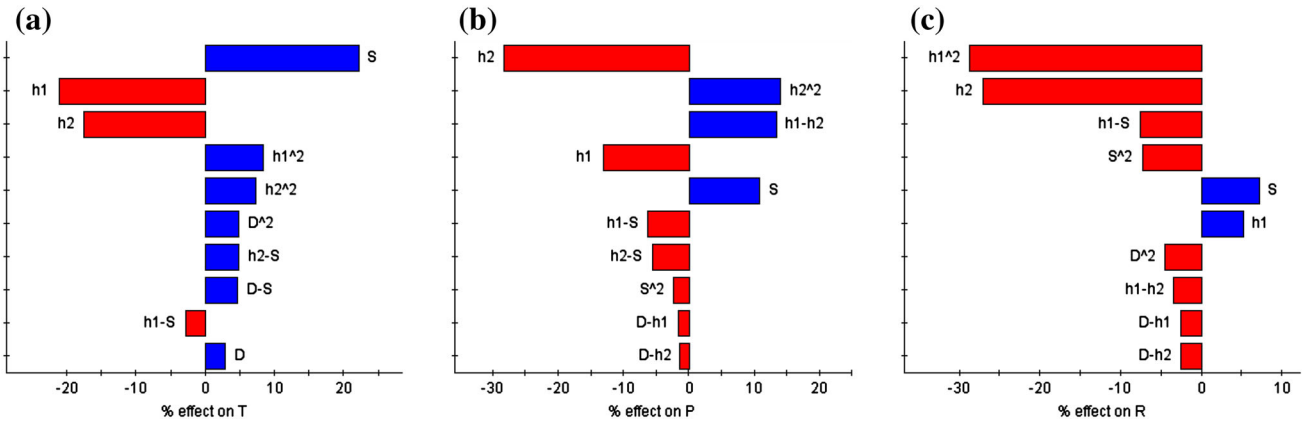

Fig. 4. Pareto plots for (a) average temperature, (b) pressure loss, (c) temperature uniformity.

Table III. Comparison of results

Case	*D*, *S*, *h*1, *h*2	T_{CFD}	T_{model}	Error	P_{CFD}	P_{model}	Error	γ_{CFD}	γ_{model}	Error
1	15,3,32,6	576.13	577.37	0.22%	1845	1852	0.38%	0.9590	0.9575	0.17%
2	15,3,14,8	584.97	585.24	0.05%	1919	1931	0.62%	0.9431	0.9462	0.33%
3	10,2,18,6	581.10	581.76	0.11%	2084	2055	1.39%	0.9603	0.9574	0.30%

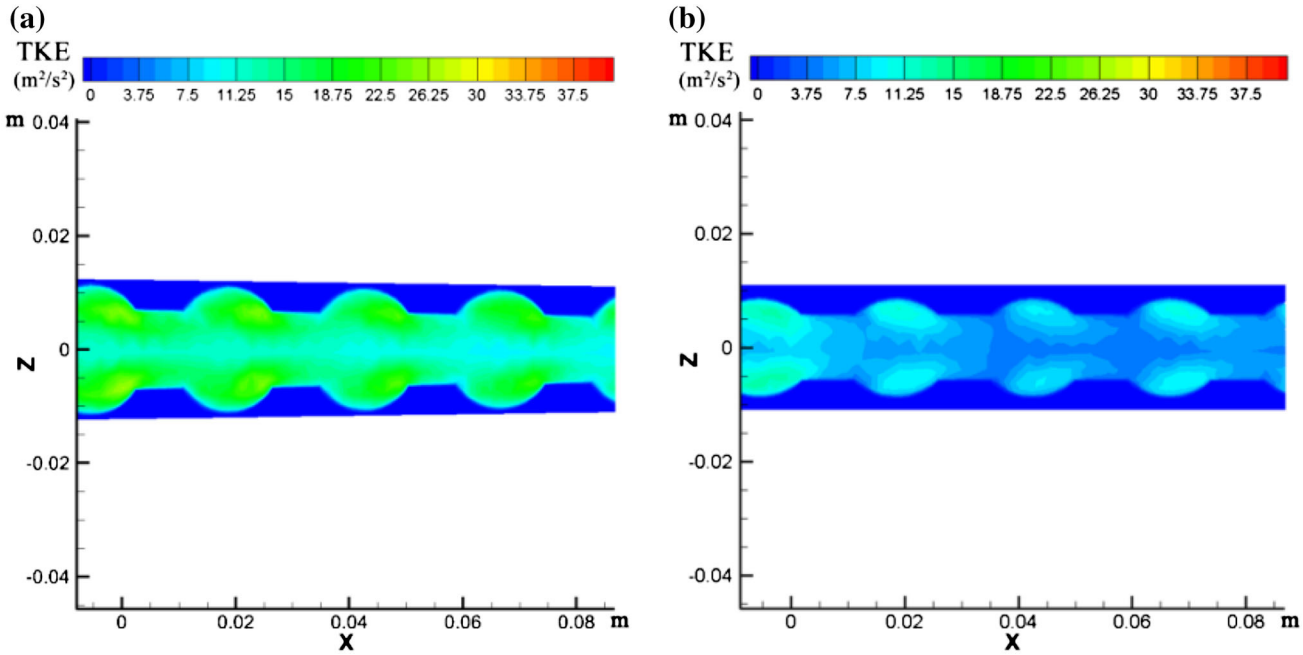

Fig. 5. Turbulent kinetic energy (*TKE*) contours on $y = 0$ (a) optimization design; (b) initial design.

multi-island genetic algorithm (GA). The chosen optimal design variables were as follows: $S = 16$ mm, $D = 4.5$ mm, $h_1 = 19$ mm, and $h_2 = 10$ mm. The temperature, pressure loss and temperature difference for the surrogate model were 581.10 K, 1738 Pa and 0.9490, respectively. By inputting the optimal design variables into the CFD simulation, the corresponding results were 581.19 K, 1757 Pa and 0.9510, respectively. Compared with the surrogate model results, the differences are only 0.02%, 1.08% and 0.20%, respectively. These results validate the precision of the surrogate model. Compared with the pressure loss and temperature uniformity of the initial heat exchanger design (S, D, h_1, and h_2 are 15 mm, 3 mm, 12 mm, and 12 mm, respectively), the

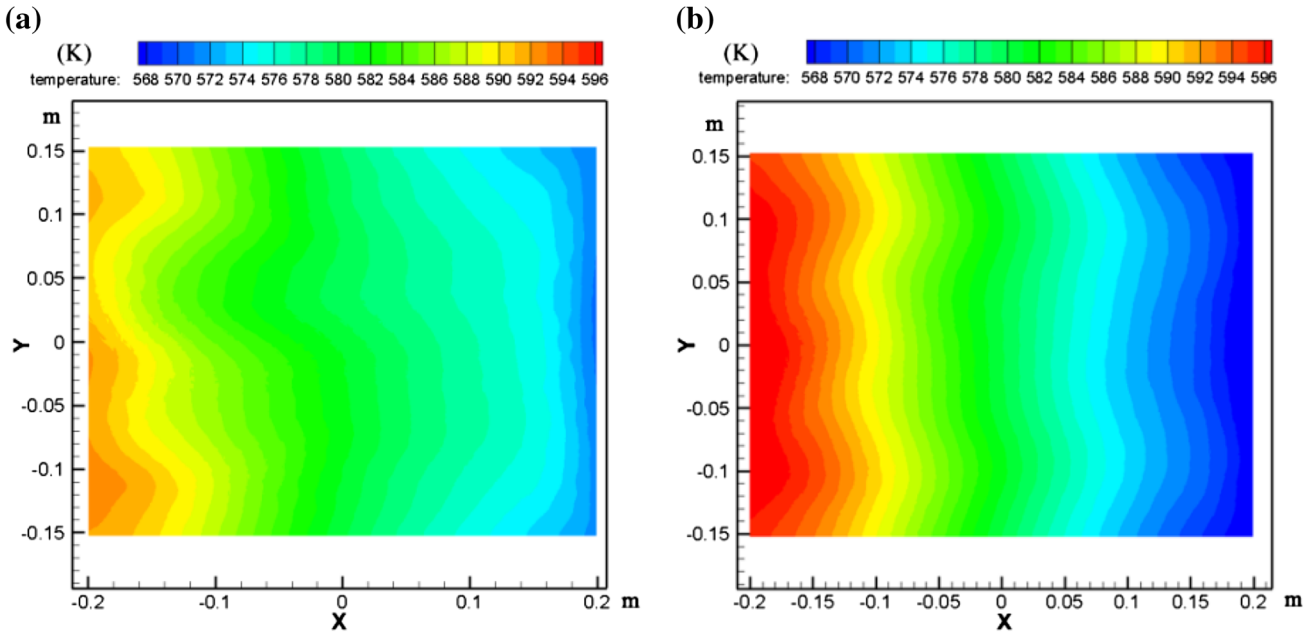

Fig. 6. Temperature distribution of (a) optimized heat exchanger; (b) initial heat exchanger.

temperature increased from 581.12 K to 581.19 K and the temperature uniformity from 0.9262 to 0.9510, corresponding to 0.12% and 2.67% respectively. The pressure loss increased from 1681 Pa to 1757 Pa. Considering that the back-pressure produced by the muffler varied from 4000 Pa to 6000 Pa, this was an acceptable cost for the temperature increasing from the lowest level to a relatively high level.

Figure 5 shows streamlines and turbulent kinetic energy (TKE) contours on the spanwise planes. The TKE value was about 20 m^2/s^2 in the optimization design which was a value double that of the initial design, while the TKE value difference along the flow direction seemed to be smaller. Therefore, with an optimization of dimples and channel height, the TKE contours were controlled and improved.

The temperature distribution of the optimized heat exchanger and the initial heat exchanger are shown in Fig. 6. The average temperature was nearly the same. By optimization, the temperature decreased on the front section and increased on the rear section, which significantly improved the temperature uniformity on the heat exchanger. The optimized heat exchanger kept the thermoelectric modules close to the same or similar working conditions which was helpful in reducing the ring current and improved the efficiency. Also, the life expectancy of each thermoelectric module could be nearly the same.

CONCLUSIONS

Taking a combination of average temperature, pressure loss and temperature uniformity as optimization goals, the optimization of a heat exchanger with a dimpled surface was conducted using the Kriging model based on CFD simulation results. It was found that the average temperature was sensitive to dimple depth D, and pressure loss and temperature uniformity were most sensitive to channel rear height, h_2. After the optimization, the temperature uniformity was significantly improved, which is helpful for increasing electric power generation. The average temperature increased from 581.12 K to 581.82 K, the temperature difference from 0.9262 to 0.9556 and the pressure loss from 1681 Pa to 1807 Pa. The TKE contours and temperature distribution were discussed, and, with an optimal design of channel structure, the temperature uniformity can be greatly improved.

ACKNOWLEDGEMENT

The research was supported by National Natural Science Foundation of China (Grant No. 51305312), National Basic Research Program of China (973 Program, Grant No. 2013CB632505) and the Fundamental Research Funds for the Central Universities (Grant No. WUT165207001).

REFERENCES

1. K. Ikoma, M. Munekiyo, K. Furuya, M. Kobayashi, T. Izumi, and K. Shinnohara, *J. Jpn. Inst. Met.* 63, 1475 (1999).
2. E.F. Thacher and B.T. Helenbrook, *Proc. Inst. Mech. Eng.* 221, 95 (2007).
3. Q. Hussain, D. Brigham, and C. Maranville, *SAE Int. J. Engines* 2, 1132 (2009).
4. J. Yang and F.R. Stabler, *J. Electron. Mater.* 38, 1245 (2009).
5. A. Sarhadi, R. Bjørk, and N. Lindeburg, *Energy Convers. Manag.* 119, 481 (2016).

6. O. Sidek and M. Ishak, *International Conference on Electrical, Control and Computer Engineering* (IEEE, 2011), p. 526.
7. J.Y. Jang and Y.C. Tsai, *Appl. Therm. Eng.* 51, 677 (2013).
8. Y.L. Zhang and M. Cleary, *Energy Convers. Manag.* 105, 946 (2015).
9. S. Kim and C. Son, *Appl. Therm. Eng.* 103, 1145 (2016).
10. D.K. Mohanty, *Biol. Bull.* 102, 228 (2016).
11. M. Cavazzuti, E. Agnani, and M.A. Corticelli, *Appl. Therm. Eng.* 84, 110 (2015).
12. S.M. Lee and K.Y. Kim, *Int. J. Therm. Sci.* 94, 1 (2015).
13. R. Quan, X. Tang, and S. Quan, *J. Electron. Mater.* 42, 1469 (2013).
14. Y.P. Wang, C. Wu, and Z. Tang, *J. Electron. Mater.* 44, 1724 (2015).
15. C.Q. Su, C. Huang, and Y.D. Deng, *J. Electron. Mater.* 45, 1464 (2016).
16. Y.C. Wang, C.S. Dai, and S.X. Wang, *Appl. Energy* 112, 1171 (2013).
17. Y.P. Wang, C. Wu, and G.F. Tan, *Proc. Inst. Mech. Eng. Part D* (2016).
18. Y.P. Wang, S. Li, and X. Yang, *Appl. Acoust.* 111, 16 (2016).
19. J. Turnow, N. Kornev, and V. Zhdanov, *Int. J. Heat Fluid Flow* 35, 168 (2012).
20. Y.P. Wang, S. Li, and X. Yang, *J. Electron. Mater.* 45, 1792 (2015).
21. M. Zhao and W.C. Cui, *J. Mar. Sci. Appl.* 6, 24 (2007).
22. K.Y. Kim and D.Y. Shin, *Int. J. Therm. Sci.* 47, 1463 (2008).
23. X. Hu, X. Chen, and Y. Zhao, *Adv. Space Res.* 53, 870 (2013).
24. Y.P. Wang, S. Li, and Y.F. Zhang, *Energy Convers. Manag.* 126, 266 (2016).